fluids

MDPI

Article

Analysis of the Evolution of Shock Waves When a Muzzle Jet Impacts a Constrained Moving Body

Zijie Li and Hao Wang *

School of Energy and Power Engineering, Nanjing University of Science and Technology, Nanjing 210016, China; lizijie@njust.edu.cn

* Correspondence: wanghao1960@126.com

Abstract: The evolution form of the flow field generated via the impact of a muzzle jet on a constrained moving body changes from the state of fully free-spatial development to that of constrained development, and it involves the problem of interference, owing to the spatiotemporal coupling of various kinds of shock waves and vortices. Against this backdrop, the authors use the dynamic mesh method to establish two models for simulating the flow field and exploring the mechanism of development and the characteristics of propagation of disturbances induced via the shock waves as the muzzle jet impacts a constrained moving body. The results show that the muzzle jet exhibited a circumferentially asymmetric shape under the influence of the constrained track. The shock wave leaned towards the upper part of the muzzle, and its speed of propagation above the muzzle was higher than that below the muzzle. Meanwhile, the vortex that should have been present below the muzzle disappeared, and it was replaced with a separation line. Changes in the pressure of the flow field and important parameters of the moving body also became more complex due to the influence of the constrained track.

Keywords: shock wave; vortex; muzzle jet; constrained track; dynamic mesh

check for updates

Academic Editor: Robert Martinuzzi

Received: 3 January 2025
Revised: 20 February 2025
Accepted: 21 February 2025
Published: 26 February 2025

Citation: Li, Z.; Wang, H. Analysis of the Evolution of Shock Waves When a Muzzle Jet Impacts a Constrained Moving Body. *Fluids* **2025**, *10*, 57. https://doi.org/10.3390/fluids10030057

Copyright: © 2025 by the authors. Licensee MDPI, Basel, Switzerland. This article is an open access article distributed under the terms and conditions of the Creative Commons Attribution (CC BY) license (https://creativecommons.org/licenses/by/4.0/).

1. Introduction

The traditional muzzle has a completely circular shape, or it is equipped in such devices as muzzle brakes of varying shapes [1,2]. However, a recently developed launch device was equipped with a long track in front of the muzzle for the non-destructive recovery of a projectile during the operation of a rocket track [3,4]. This leads to a unique form of motion for the projectile. That is, the movement of the projectile changes from high-speed motion in an open, full space to constrained high-speed motion. This renders the characteristics of transient development of the moving shock wave in this novel muzzle jet significantly different from those in the traditional muzzle jet.

The muzzle jet poses a series of aerodynamic problems in which such complex flows as shock waves/shock wave interference, a strong moving shock wave, and strong vortices represent the major phenomena of flow in the flow field [5–7]. The shock wave in the conventional muzzle develops in a free field in full space, and it is spherically symmetric in three dimensions (3D). Compared with the traditional muzzle jet, the projectile moves forward on the track as propelled by this novel type of muzzle jet to form a special moving boundary at a right angle with the track, where this constrains the development of the muzzle jet in free space. The muzzle jet subsequently exhibits highly 3D, circumferential, and asymmetric characteristics that lead to the formation of multiple types of vortices [8]. The development of the muzzle jet thus becomes complex under the interference of the

track. It is, therefore, important to analyze the complex phenomena of flow in muzzle jets with restricted boundaries to inform scientific research in the area and solve key technical problems [9,10].

A considerable amount of research has been devoted to the muzzle jet, and it has led to the establishment of a relatively systematic theory. The characteristics of the transient evolution of shock waves caused by interference with the muzzle device, and the impact of the muzzle jet on a high-speed moving body in full space, have long been popular subjects of research in this area [11,12].

Schmidt et al. [13,14] measured the characteristic parameters of a set of muzzle brake structures by using a 20-mm small-caliber gun, and they obtained clear images of the muzzle jet. They analyzed the characteristics and flow mechanism of the muzzle jet, and they observed that the coupling between the flow fields along the axial direction was very strong but that along the transverse direction was very weak.

Zeqing et al. [15,16] conducted a systematic study of the flow field of a 7.62-mm small-caliber launcher with a cylindrical muzzle device impacting a high-speed projectile in full space. The results showed that the vorticity in the flow field was mainly concentrated at the boundary of the jet, and a large number of small-scale vortices appeared downstream of the Mach disk. As the bottle-shaped shock wave contracted, the vortex ring above the three wave points detached from the boundary of the jet and developed independently. Instability subsequently occurred at the boundary, and this led to the formation of a large number of large-scale vortices directly downstream of the Mach disk. The jet inside the muzzle was much more complex under the influence of the muzzle device (cylindrical nozzle).

Huanhao et al. [17,18] used large-eddy simulations to examine the characteristics of the flow field during the interaction between a supersonic mainstream and a transverse jet, and they used the results to derive the law of evolution of the morphology of the 3D shock wave. The leading edge of the jet formed a bow-shaped shock wave and a separated 'λ' shock wave, owing to the strong inverse pressure gradient formed via the interaction between the supersonic mainstream and the transverse jet. In addition, the interaction between the strong compression-induced shock wave, the shear layer, and the horseshoe vortex accelerated instability in the flow field, and this resulted in the formation of a complex multi-scale structure of the downstream flow. Therefore, the complex shock wave system in the flow field of the supersonic transverse jet plays an important role in inducing turbulence in it, as well as strengthening the mixing between the jet and the mainstream.

Zijie [19,20] identified the evolution characteristics of the shock wave of muzzle jets in case of an initial interference with the jet. The velocity of the shock wave increased in the muzzle jet subjected to this interference, and it led to more pronounced wrapping of the moving projectile. This led to a strengthening of the effect of the shock wave at the bottom of the muzzle jet, and it hindered the generation of the Mach disk.

Zijie, Wang Hao [21] conducted experiments and numerical simulations on a 300 mm caliber balanced gun and obtained the development process and laws of a muzzle jet in near-Earth space. Research has found that muzzle shock waves reflect off the ground, forming shock waves with opposite propagation directions. The shock wave generated via ground reflection intersects with the muzzle shock wave, forming a new wavefront. A vortex was generated near the new wavefront, and the shape of the shock wave at the bottom of the projectile was also disrupted, exacerbating the initial disturbance of the moving projectile.

The above brief summary of the literature shows that researchers have extensively examined the characteristics of the flow field of a muzzle jet impinging on a moving body in a free state and half-space from the perspectives of mechanisms, numerical simulation methods, and visualization experiments. But few studies have investigated the develop-

ment and evolution of shock waves and vortices when the muzzle jet impacts a constrained moving body. This is a new scientific problem that has important guiding significance for solving the key technical difficulties in the engineering application of integrated gun rocket sled launch systems. Therefore, it is necessary to conduct research on the development and evolution mechanisms of various forms of shock waves and vortices in the flow field of jet impact-constrained moving bodies. Accordingly, the authors of this study establish a representative model of simulation with the FLUENT software 2019R1, which utilizes a k–ε turbulence model and combines it with dynamic grid technology. At the same time, we compile the six degrees of freedom of the moving body for the secondary development of the software to examine the evolution characteristics of the shock wave of a supersonic jet as it impacts a constrained high-speed moving body. We identify the process of transient evolution of shock waves in the flow field by combining theoretical calculations, simulations, and experiments.

The remainder of this article is structured as follows: Section 2 provides a detailed introduction to the physical model, the model of the mesh, the dynamic mesh method, boundary conditions, and the methods of solution. We also report the results of tests in that section. Section 3 discusses the evolution characteristics of the shock wave when a supersonic jet impacts a constrained moving body, including the structure of the muzzle jet, the evolution of the shock wave, the generation and evolution of vortices, the transient changes in the pressure at key points, and the differences in the key parameters of the moving body. Section 4 summarizes the conclusions of this study.

2. Physical Model and Mesh Model

2.1. Physical Model

To clearly represent the development and evolution of shock waves when the muzzle jet impacts a constrained moving body, where this is different from cases involving traditional muzzle jets, we established two models of numerical simulation: one without a constrained track in front of the muzzle (Case 1) and the other with it (Case 2). Except for the presence/absence of the constrained track, all other parameters of the two models were identical. We focus here on the structures and sizes of the inlet of the jet and the moving body. Figure 1a–c show the overall structural diagram of the proposed model, and schematic diagrams of the models without the constrained track (Case 1) and with it (Case 2), respectively. The model included a constrained track, a tube, a moving body, and support plates. Its dimensions were set according to the parameters of the corresponding experiments conducted by the authors, and its size-related parameters are shown in Table 1. The diameter of the muzzle *Dm* was 65 mm, and the length of the moving body *Lb* was 200 mm. The size of the entire computational domain *Lx* was 5.7 m along the direction of motion of the body, which moved over a distance, *Li*, of 5 m. The lengths *Ly* and *Lz* of the computational domain were 2.5 m. Due to its structural design, the new muzzle of the launch device was not completely circular but had a shape that conformed to that of the constrained track. The moving body also had a corresponding shape. The cross-sectional shape of the track is rectangular. The height is 200 mm, and the width is 25 mm. In this article, numerical simulations were conducted on half of the physical model with a width of 12.5 mm. The length fully satisfies the length of the physical model in the direction of projectile motion.

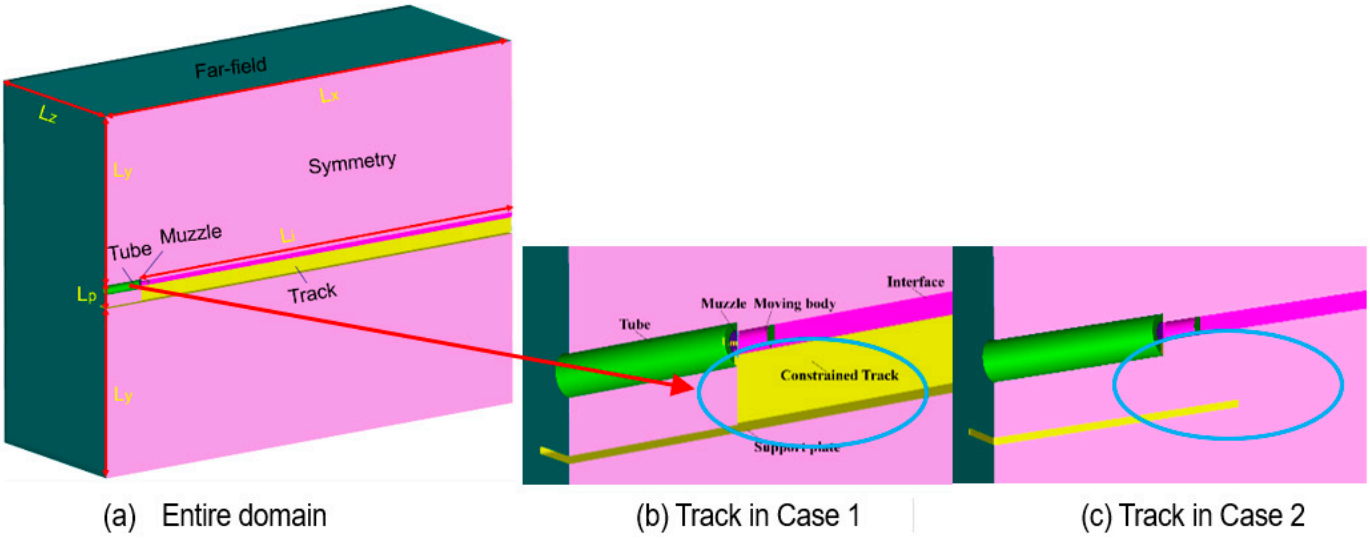


Figure 1. Simulated physical structures of the computational domain and the track.

Table 1. The size-related parameters of the model.

Parameter	Value
Lx	5.7 m
Ly	2.5 m
Lz	2.5 m
Dm	65 mm
Lb	200 mm
Lp	255 mm
Li	5.0 m

2.2. Meshing Method

To reduce the cost of calculations and the time needed to perform them, we conducted simulations on only half of the models considered here (as shown in Figure 2). The computational domain was divided into approximately 9.8 million structured grids. When simulating a complex flow field, it is often difficult to generate a single, high-quality structural grid. Moreover, the simulations required the dynamic grid method, which made it necessary to divide the entire computational domain into subdomains of stationary and dynamic grids for processing. The interface was used for numerical exchange.

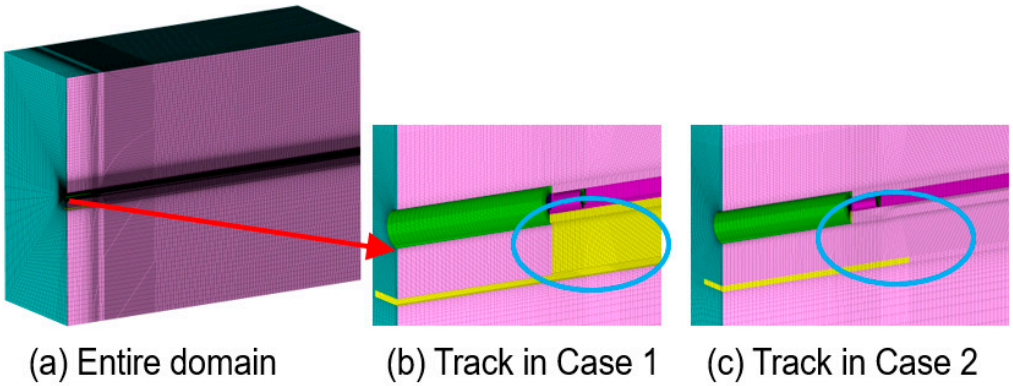


Figure 2. Schematic diagram of the model of the grid.

2.3. Dynamic Mesh Method

We needed to use dynamic grid technology to handle the changes in the grid caused by the motion of the body during the calculations. The dynamic grid method based on three algorithms was used to calculate the requisite adjustments to the internal nodes of the grid: the layering, smoothing, and remeshing algorithms. Because we assumed that the body moved only in one direction, it was appropriate to use the layering method to simulate its motion. The layering method mainly uses a pair of interfaces for data transfer. The interface is mainly used to handle the data transfer between region interfaces in multi-region computing models. Therefore, in order to keep the computing domain smooth in multi-region computing models, interfaces need to be created at the boundaries of mutual contact. Meanwhile, this method requires setting the segmentation and merging factors of the mesh. The mesh behind the body shifted forward along the x-axis due to the motion of the projectile. A layer of the mesh near the muzzle was thus elongated and had a side length of hs. The part of the mesh that exceeded the boundary of the computational domain was truncated, and the length of the layer of mesh near the boundary of the computational domain was hc. Assuming that the ideal size of the mesh was hi, we divided it into two parts when the size of the newly generated mesh satisfied h > (1 + Cs) hi. When the size of the mesh satisfied the condition h > Cshi, the grid was merged into a single grid. In this example, hi = 2.0 mm, Cs = 0.4, and Cl = 0.2.

2.4. Boundary Conditions and Solution Methods

We simulated the model of a supersonic jet impinging on a high-speed moving body in Fluent software 2019 R1. Figure 3 shows the types of boundaries used in the simulations. The outlet of pressure was set as the boundary condition of the domain of calculation, while the tube and track were assumed to be non-sliding insulated walls. The moving body was assumed to adhere to the boundary condition of the moving wall, and it was controlled via a user-defined function (UDF) with six degrees of freedom (6 DOFs). The initial velocity was set to 500 m/s according to the results of prior experiments. The inlet of pressure was set as the boundary condition for the muzzle, and it was 45 MPa, according to the experiments. The environmental pressure was 101,325 Pa, and the temperature was 300 K.

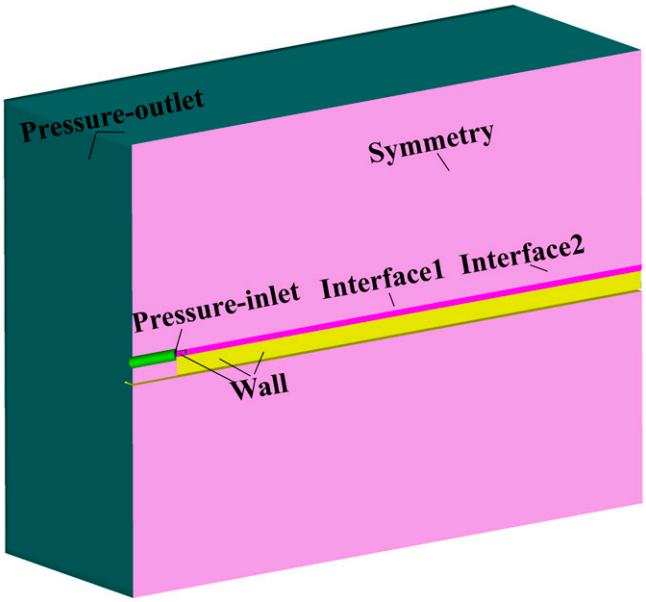


Figure 3. Boundary conditions of the model of the muzzle jet.

We processed the motion of the body in the block-based division of the mesh by using the finite volume method in combination with the structural dynamic method. The

Navier–Stokes (N–S) equation solver based on density correction and the k-ε realizable model of turbulence was used. The inviscid convective flux was split by using the Roe-FDS scheme, and the implicit scheme was used with the time-marching method to accelerate the convergence of the numerical calculations. The equation of flow control was discretized using the second-order upwind scheme, and the material was assumed to be an ideal gas.

2.5. Test Verification

These simulations were based on a small-scale experiment conducted by the authors. Due to constraints imposed by the experimental equipment and the conditions of implementation, the constrained track was short, such that it might have skewed the results of the experiment. The experimental platform is the main jet generator, which ignites the gunpowder inside the gun barrel through an ignition device, generating high-temperature and high-pressure gas to launch the moving body. The PEPE KD2002L-02 free field pressure sensor is used, with a measurement range adjustable from 1–10 MPa, to monitor the pressure changes in key characteristic points in front of the muzzle over time. The signal is collected using the DEWE2-A13 transient data recorder produced by DEWETRON Industrial Equipment Company in Austria. Figure 4 is the experimental platform involved in this article; the schematic diagram of the experimental plan and the measuring device are shown in Figures 5 and 6.

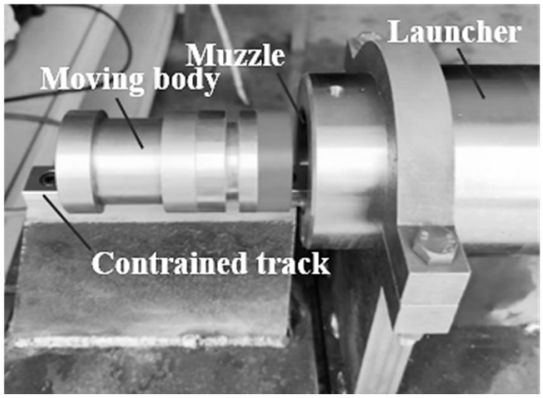


Figure 4. Experiment platform of the nozzle of the engine used for the rocket track test.

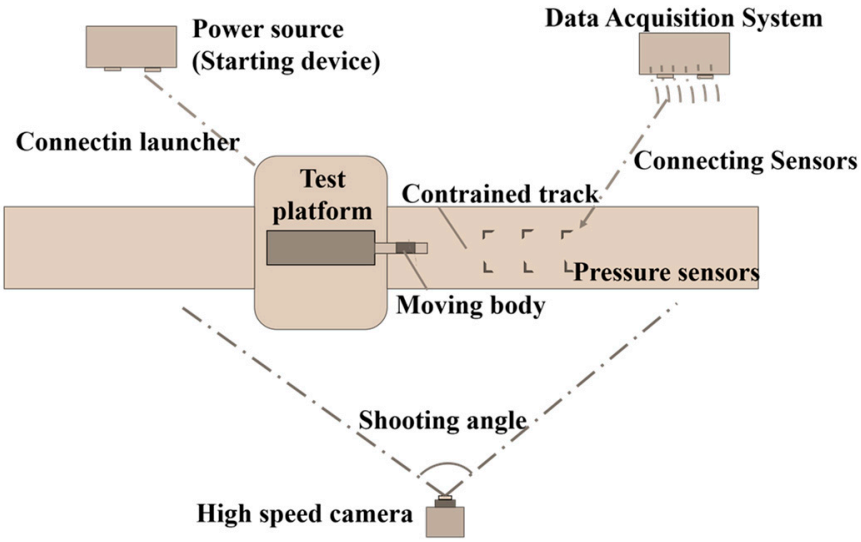


Figure 5. The schematic diagram of the experimental plan.



Figure 6. The measuring device of the free field pressure sensor.

We verified the experiments based on numerical simulations, and subsequently mainly analyzed the model of numerical simulation in this study. Figure 7 compares the changes in pressure over time between the experiment and the simulation at the key monitoring point (1500, 30, and 10) mm, and it is evident from it they were consistent. Therefore, the method of simulation and the mesh used in this article could accurately represent the characteristics of the muzzle jet.

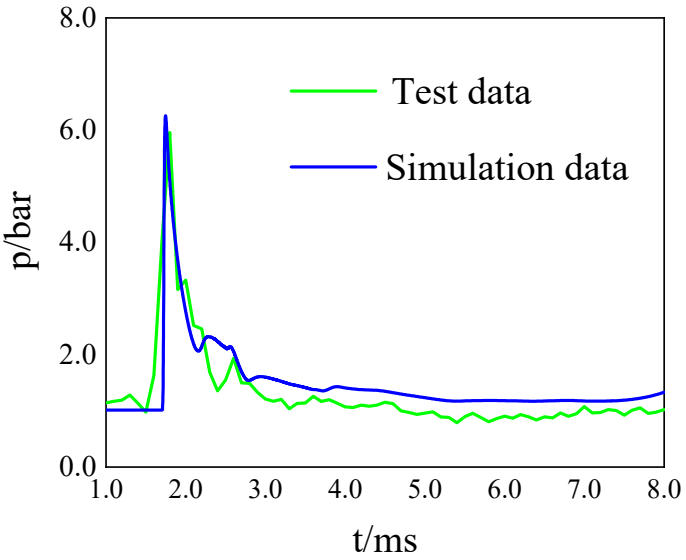


Figure 7. Comparison of pressure between the results of the experiments and simulations.

2.6. Grid Independence Verification

We provide three sets of grids, which are defined as coarse mesh, fine mesh, and dense mesh, with 6 million, 9.8 million, and 12 million, respectively. The numerical simulation results of different grid models considered for the thrust variation on the bottom of the moving body in Case 1 are shown in Figure 8. As the figure shows, the results obtained using fine mesh and dense mesh are very close, with an error of less than 1%. On the contrary, there are significant differences in the results obtained from the coarse grid model.

Therefore, it can be concluded that, when using a fine mesh model, the simulation results are independent of the mesh size.

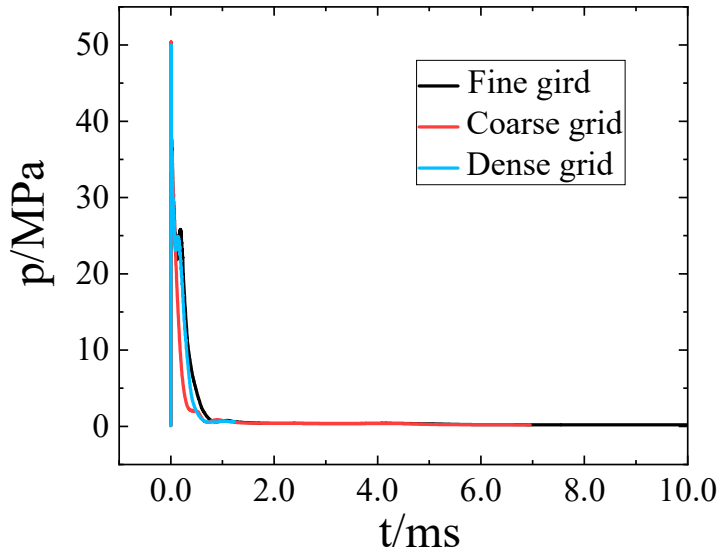


Figure 8. The thrust variation on the bottom of the moving body for grid independence verification.

3. Analysis of Results

We aim to analyze the evolution of shock waves in the muzzle jet under different boundary conditions. The process of interest includes the development of shock waves in the muzzle, the structure of vortices generated by them, and the flight attitude of the moving body. In view of this, we examine the characteristics of the development of flow in the muzzle jet on a symmetric plane, the development and evolution of vortex structures in the flow field, changes in pressure at symmetric monitoring points, and the key parameters of motion of the body in the two models considered here.

3.1. Analysis of Muzzle Jet

We monitored the contours of pressure at different times to compare the models of the muzzle jet with and without constrained tracks. We do not provide more details on the conventional muzzle jet because past studies have already reported a sufficient amount of research on it [2,22]. Figures 9 and 10 show the contours of pressure on the plane of symmetry in Case 1 and Case 2 from 0.5–5 ms. It is clear from them that the muzzle jet differed significantly in the two models.

Figure 9 shows the preliminary structure of the flow field of the muzzle in Case 1. The muzzle jet emitted high-temperature and high-pressure gas, which then rapidly expanded. As its pressure decreased, the velocity of the gas increased. It subsequently spread and pushed the air around the muzzle to form a spherical shock wave. The muzzle jet had a roughly circumferential symmetric structure because the muzzle was not a complete circle. The muzzle jet developed much more quickly at the junction of the trajectory of the muzzle, where this was also the local minimum cross-section. However, the development of the flow field of gas was insufficient, such that it influenced only a small portion of the area. Nonetheless, typical muzzle jets remain adequately representative.

The shock wave at the muzzle continued to develop over time, and the scope of its impact gradually expanded. Figure 9b,c show that the muzzle jet developed gradually, and its asymmetry decreased over time. A complete wave system consisting of a multi-level shock wave, which was composed of coronal shock waves, reflected shock waves, Mach disks, and overlapping discontinuities, was formed around the muzzle. It is clear from Figure 9d–f that the muzzle jet developed thoroughly, and it had an axisymmetric shape.

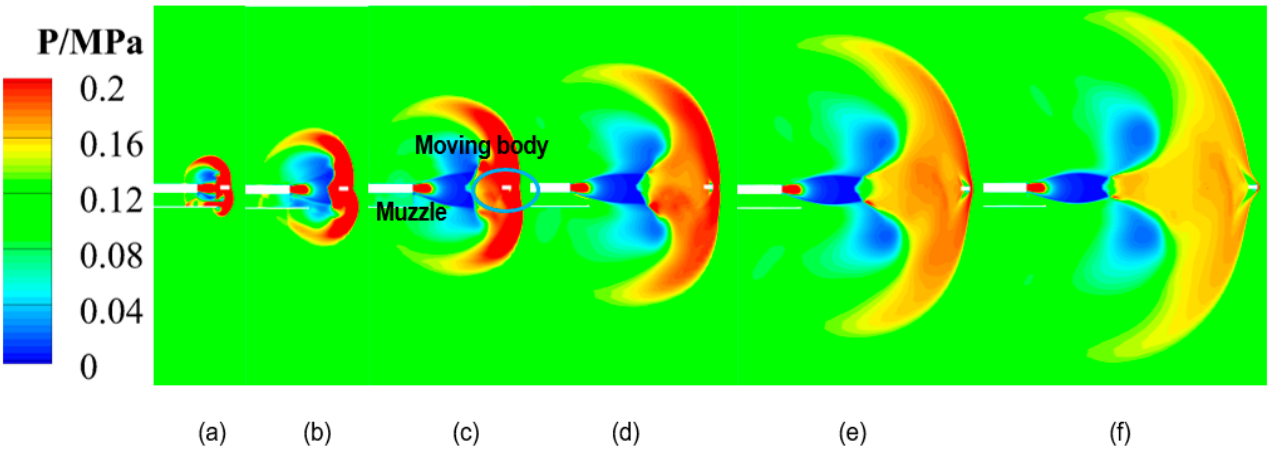


Figure 9. Contours of pressure of the muzzle jet on the plane of symmetry over time in Case 1: (**a**) t = 0.5 ms; (**b**) t = 1.0 ms; (**c**) t = 2.0 ms; (**d**) t = 3.0 ms; (**e**) t = 4.0 ms; (**f**) t = 5.0 ms.

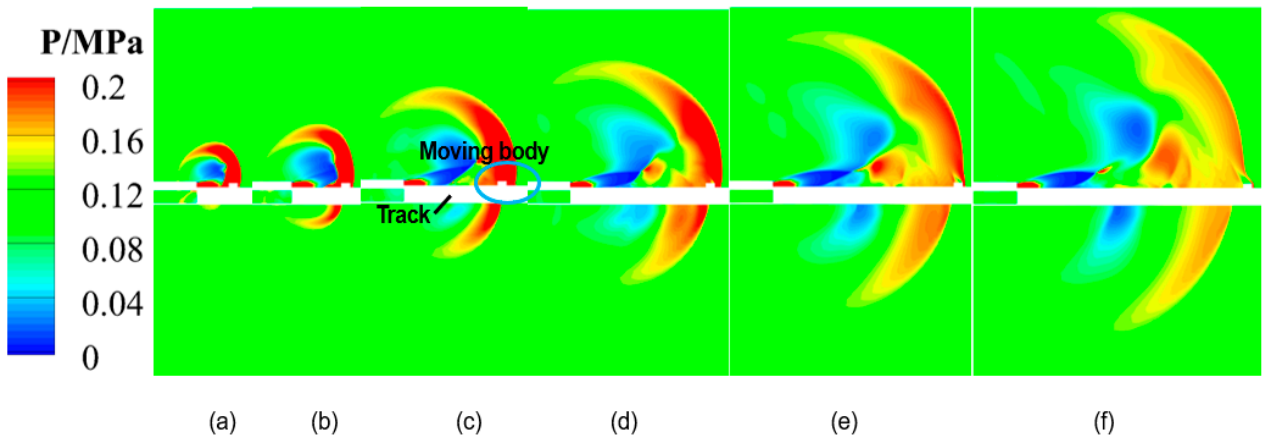


Figure 10. Contours of pressure of the muzzle jet on the plane of symmetry over time in Case 2: (**a**) t = 0.5 ms; (**b**) t = 1.0 ms; (**c**) t = 2.0 ms; (**d**) t = 3.0 ms; (**e**) t = 4.0 ms; (**f**) t = 5.0 ms.

The flow fields of the two models exhibited certain differences, owing to their different tracks. The track cut-off space for the downward development of the muzzle jet in Case 2, causing it to twist and deform while exhibiting a highly asymmetric axial shape. The flow field was no longer a spherical wavefront, and this hindered its development. Therefore, the shock waves needed to bypass the track in order to continue propagating. They were reflected at this point such that this caused another shock wave to form in the opposite direction of propagation, thereby forming a corresponding wavefront along the track. The track prevented the shock wave from propagating downwards, and it was reflected and propagated upwards to form an irregularly shaped wavefront. On the whole, it developed in 3D space in the area above the track.

Figure 10a shows that high-temperature and high-pressure gas was ejected from the muzzle along the constrained track, and it influenced only the area above the track, owing to the insufficient development of the muzzle jet. Figure 10b shows that the shock wave influenced the lower area of the constrained track over time, and the body moved forward on the track. It is clear from Figure 10c,d that the coronal shock wave in front of the moving body was significantly asymmetric, and its speed of propagation in the upper region was significantly higher than that in the lower region. The Mach disk was also truncated by the track, such that it was incompletely formed. Figure 10e,f show that the muzzle jet had fully developed, with a prominent decrease in its asymmetry. The development of the flow field was dependent on its previous states, and it featured asymmetric coronal shock waves,

reflected shock waves, multi-level shock waves composed of Mach disks, and a complete wave system of overlapping discontinuities that had formed around the muzzle.

3.2. Analysis of Vortices

To further compare the muzzle jets with differently constrained boundaries, we analyzed the development of vortex structures in the range of 1.0–4.0 ms. The presence of the track hindered the development and propagation of the shock waves in the muzzle, changed their direction of propagation, and generated lateral airflow that led to changes in the vortex structure in the muzzle jet. The vortex increased the energy consumption and diffusion of the flow field, and it influenced the distributions of its pressure and velocity. The eddy currents moved, deformed, merged, paired, and ruptured, and remained far downstream as their strength gradually decreased. The change in the vortical structure was a phenomenon unique to the muzzle jet with constrained boundaries, and it was not observed in the traditional muzzle jet. We thus focus here on the generation and evolution of vortices in the flow field.

Figures 11 and 12 show the evolution of vortices in the symmetric muzzle jet in the two cases considered here over time. Figure 11a shows that two symmetrical vortices were formed in the conventional muzzle jet over time. These vortices were located in the low-pressure zone, with the streamline directed from the center of the vortex to outside it. This means that the spiral point was stable and difficult to dissipate. The vortices developed steadily over time.

In comparison with the above, it is evident that the vortical structure in Case 2 differed significantly from that in Case 1 due to interference by the constrained track, support plate, and test platform. The vortex above the muzzle in Case 2 was similar to that in Case 1, and it was located in the low-pressure zone. Its streamline pointed outward from the center of the vortex, where this showed that the spiral point was stable, and it was difficult to dissipate. No vortex was formed in the area below the track, and the separation line was generated instead. This is because the track hindered the development of the muzzle jet above it and changed its pattern of development. The vortex is a rotating flow formed in a fluid, which can cause energy loss, fluid instability, and turbulence in the flow field. Therefore, eliminating vortices is of great significance for optimizing fluid motion and improving flow field stability. If the vortex structure in the fluid is easily dissipated, the vortex intensity in the flow field will be smaller, and the vortex dissipation rate will be higher. In this article, in models without constrained tracks, vortices are relatively stable, while in models with constrained tracks, vortices are relatively unstable. This indicates that constraining the orbit leads to a more unstable flow field, making the flow more complex and energy dissipation severe.

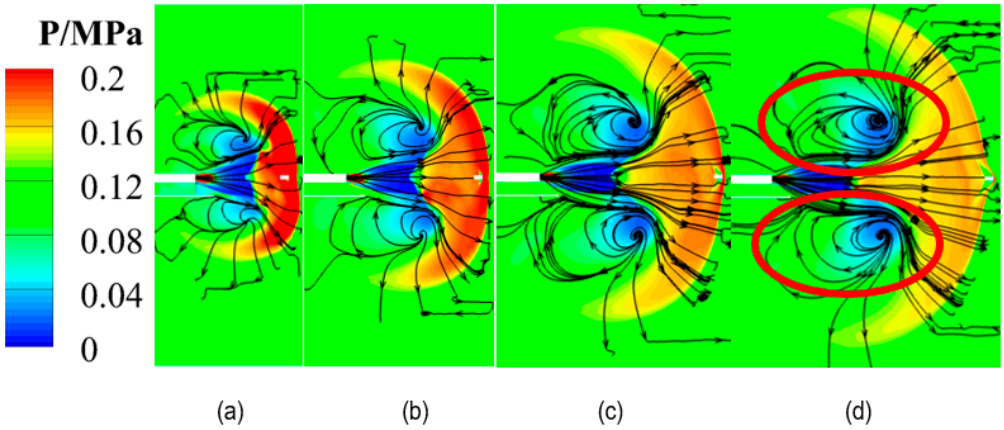


Figure 11. Contours of vortices of the muzzle jet on the plane of symmetry over time in Case 1: (**a**) t = 1.0 ms; (**b**) t = 2.0 ms; (**c**) t = 3.0 ms; (**d**) t = 4.0 ms.

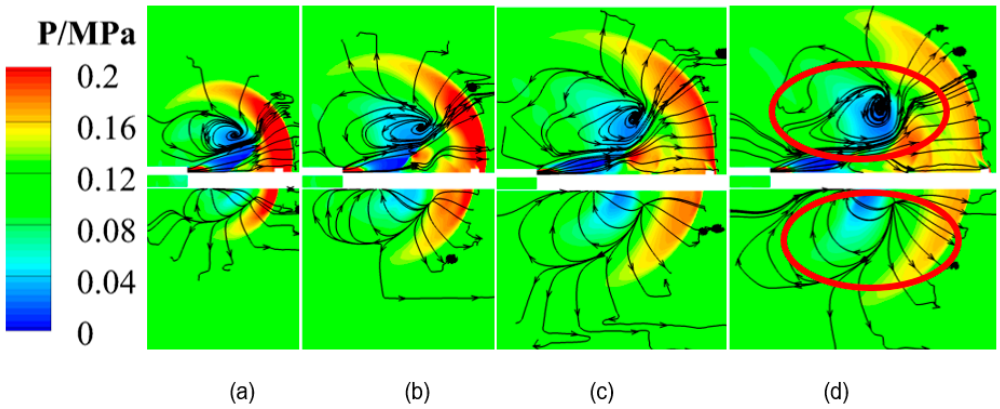


Figure 12. Contours of vortices of the muzzle jet on the plane of symmetry over time in Case 2: (**a**) t = 1.0 ms; (**b**) t = 2.0 ms; (**c**) t = 3.0 ms; (**d**) t = 4.0 ms.

3.3. Analysis of Pressure Changes

We also monitored changes in pressure at key points over time to illustrate the impact of the constrained track on the muzzle jet. Figure 13 provides a schematic diagram of the locations of the monitoring points and Table 2 shows their specific locations.

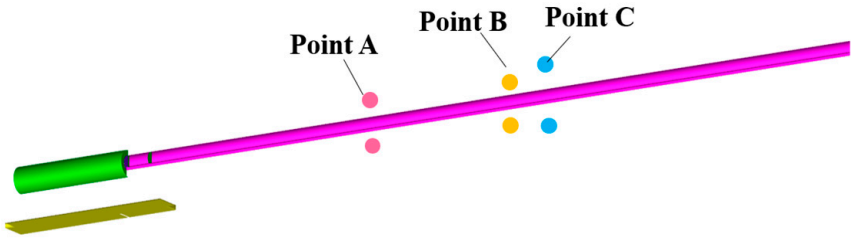


Figure 13. Distribution of the monitoring points on the track.

Table 2. Locations of the monitoring points.

Point	Location Parameter (x, y, z)/mm
A-above	(1900, 30, 100)
A-below	(1900, 30, −100)
B-above	(3000, 60, 100)
B-below	(3000, 60, −100)
C-above	(3500, 70, 200)
C-below	(3500, 70, −200)

Figure 14 shows a comparative analysis of changes in the pressure at the monitoring points considered. It is clear from it that the changes in pressure, which should have remained the same as before, now differed due to the influence of the track. When the shock wave did not propagate to a given monitoring point, the pressure at this point was assumed to be the environmental pressure. When the wavefront of the shock wave propagated to this point, the pressure at it rose. The gas continued to expand, and pressure at the relevant monitoring point decreased and finally became stable.

The shock wave is a complicated system containing alternating expansion- and compression-induced waves, where this makes it difficult to identify changes in the pressure. A comparison of the pressure between the upper and lower symmetrical points in Case 1 showed that the changes in pressure at these points were almost identical. The reason for the difference is to control a single variable; that is, although there is no constrained

track, the shape of the muzzle still maintains the same shape as in Case 2, which is not a complete circle. Therefore, it is reasonable for the pressure to have been slightly different at the upper and lower points of symmetry.

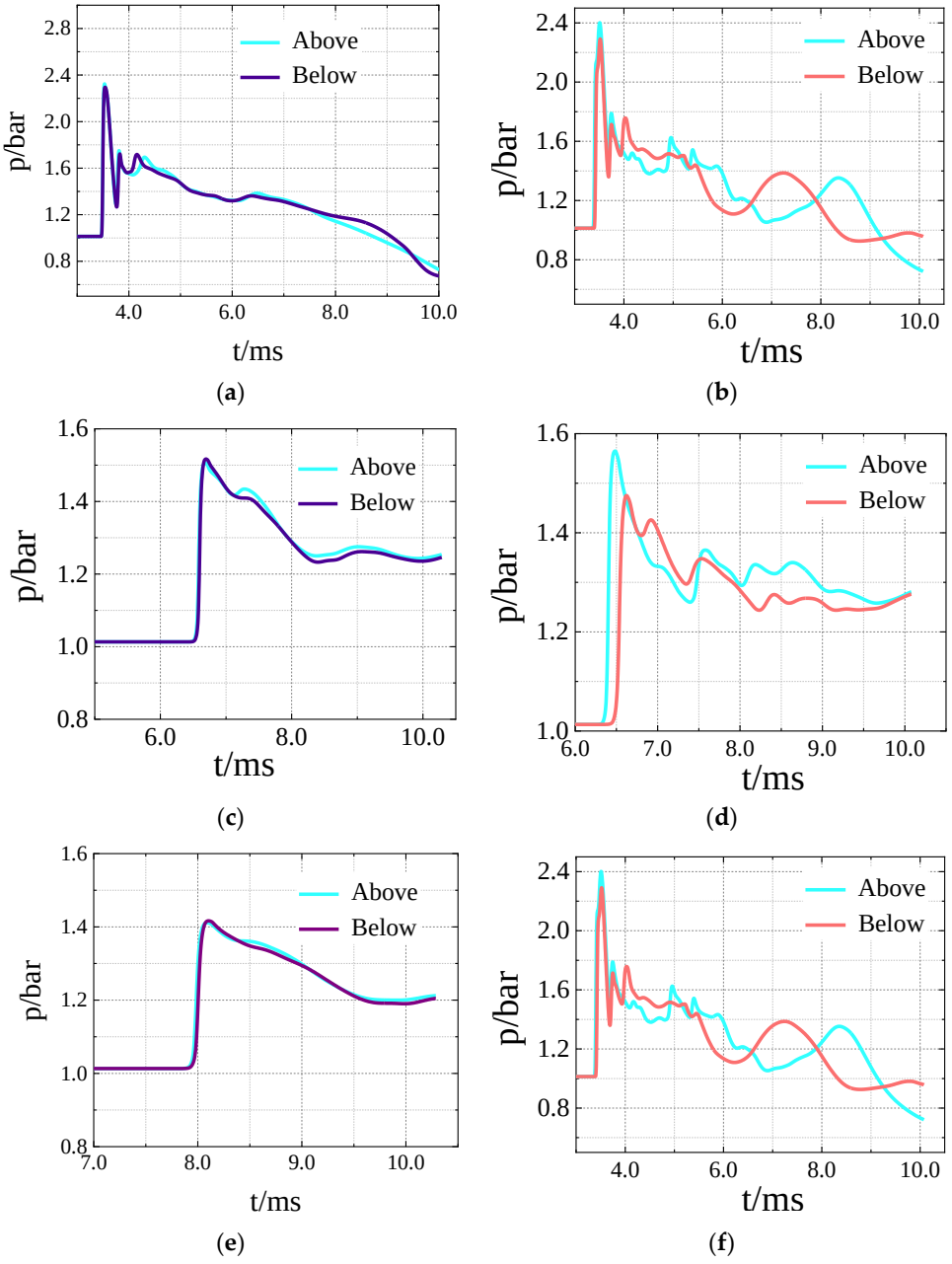


Figure 14. Pressure changes at monitoring points: (**a**) Point A for Case 1; (**b**) Point A for Case 2; (**c**) Point B for Case 1; (**d**) Point B for Case 2; (**e**) Point C for Case 1; (**f**) Point C for Case 2.

Figure 14a,b show that the trends of changes in pressure remained similar between the cases. The body moved at about 500 m/s. The shock wave moved to this point at approximately 3.8 ms, and the disturbance in pressure was observed immediately. It rapidly increased and then gradually decreased. Due to the influence of the track in Case 2, the muzzle jet deviated upwards, and this led to a higher maximum pressure at A-above than that at A-below. The pattern of development of the shock waves also became more complex, because of which the severe fluctuations in pressure during the descending stage were also significantly different from those in Case 1.

Similarly, it is clear from Figure 14c,d and Figure 14e,f that the shock wave moved to this characteristic point at approximately 6.5 ms. The change in pressure at the upper monitoring point occurred earlier than at the lower monitoring point, indicating that the shock wave tended to develop above the muzzle. Meanwhile, the maximum pressure at the upper monitoring point was higher than that at the lower monitoring point. The pattern of development of the shock waves was also relatively more complex, such that the pressure oscillated severely during the descending phase.

In addition, Figure 15 provides a comparison of the changes in pressure over time between the cases at the same monitoring point. It is clear from it that the two cases had similarities, as well as differences. The speed of propagation of the shock wave in Case 2 was higher than that in Case 1 in all Figures, indicating that the presence of the constraining track had increased the speed of propagation of the shock wave. The figures show that the variation in pressure at the characteristic point in Case 1 was relatively smooth and singular, while that in Case 2 was complex. This proves that the constrained track increased the complexity of the development of the shock wave.

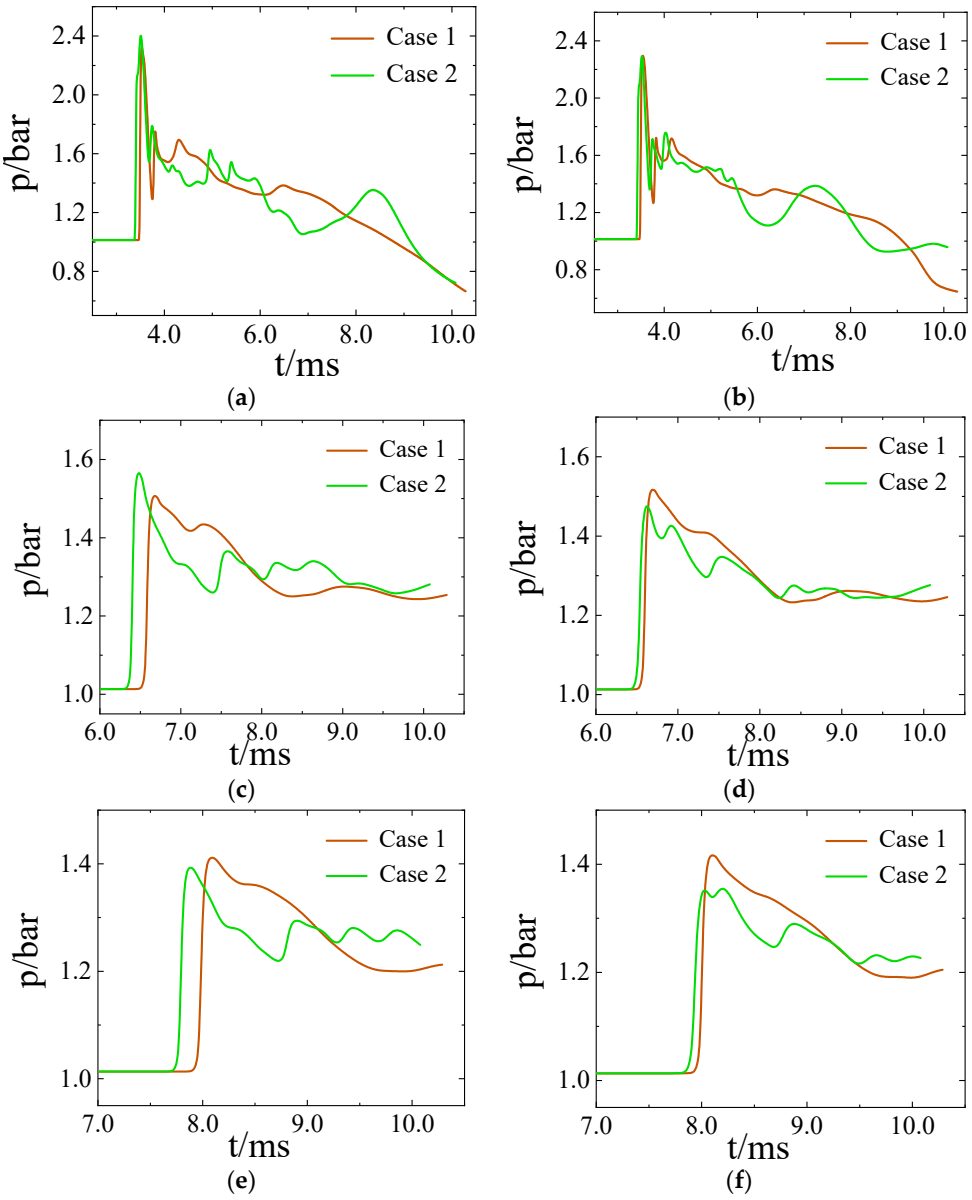


Figure 15. Pressure changes at monitoring points: (**a**) A—above; (**b**) A—below; (**c**) B—above; (**d**) B—below; (**e**) C—above; (**f**) C—below.

Specifically, Figure 15a–e show that changes in the initial pressure in Case 2 occurred much earlier than in Case 1, indicating that the speed of propagation of the shock wave in Case 2 was significantly higher than that in Case 1. These three points were all located above the muzzle, and this verifies that the constrained track caused the shock wave to develop above the muzzle.

It is clear from Figure 15b,d,f that the initial pressure in Case 2 changed slightly earlier than in Case 1, indicating that the speed of propagation of the shock wave in Case 2 was slightly higher than that in Case 1. These three points were all located below the muzzle, and this shows that the constrained track caused the speed of propagation of the shock wave in the lower region to still be higher than that in the model without the constrained track.

3.4. Analysis of Key Parameters of Moving Body

Figure 16 compares the key parameters of motion of the body. Figure 16a shows the Mach number of the moving body, while Figure 16b shows the drag on it. It is clear from Figure 16a that the Mach number of the moving body in Case 2 was higher than that in Case 1. The Mach numbers of the moving body in the two cases were very similar close to the muzzle, owing to the dominant influence of the thrust of the muzzle jet. The body gradually moved away from the muzzle, whose effect of thrust rapidly decayed. The Mach number of the moving body was more significantly influenced due to interference via the track in this case. In conjunction with the above results, it is evident that the shock waves developed more quickly in Case 2, and the Mach number of the moving body was also higher than in Case 1.

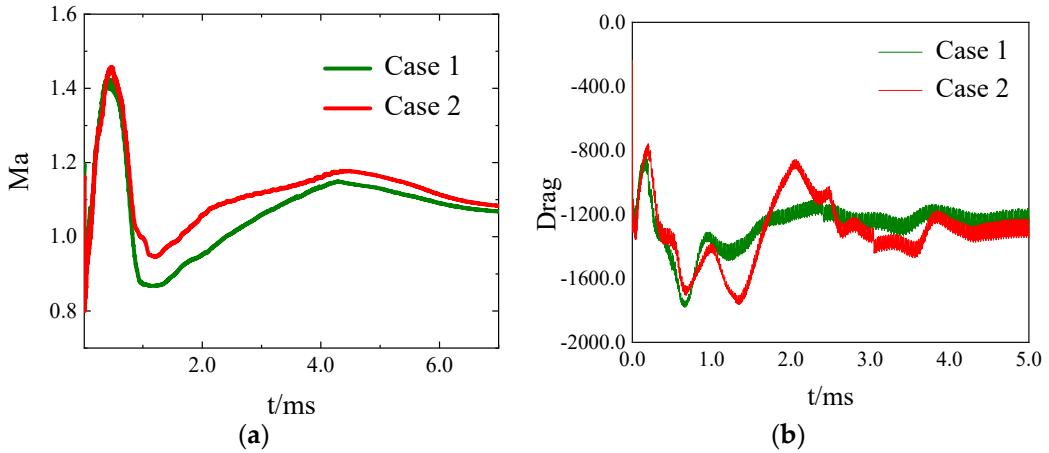


Figure 16. Mach number and drag force of the moving body: (**a**) Mach number; (**b**) drag force.

Figure 16b shows that fluctuations in resistance in Case 2 were significantly more complex than in Case 1. Because the thrust had the major influence on the muzzle jet close to the muzzle, the values of resistance of the moving body in both cases were similar. The body gradually moved away from the muzzle, and the effect of the thrust of the muzzle decayed rapidly. The change in the resistance of the moving body was significantly influenced by its speed and the track. It is also evident that the change in resistance in Case 1 was relatively smooth because the moving body flew freely in fully open space. On the contrary, the form of development of the shock wave was significantly influenced in Case 2, and it led to significant fluctuations in the resistance of the moving body.

4. Conclusions

In this study, the authors established two models of simulation to investigate the impact of a muzzle jet on a constrained moving body based on dynamic grid technology, with the aim of discussing the unique development and evolution of the shock waves and vortices. We drew the following conclusions:

(a) The presence of the constrained track led to the twisting and deformation of the shock wave of the spherical muzzle, where this should have been circumferentially symmetric. The overall shock wave leaned towards the upper part of the center of the muzzle, and its speed of development above the muzzle was much higher than that below it.

(b) The influence of the constrained track on the muzzle jet led to the generation of lateral airflow that influenced the morphology of the vortices. The vortices were supposed to be symmetrical above and below the muzzle. However, the vortex above the muzzle became asymmetrical, and that below it disappeared. Only a separation line was formed below the muzzle.

(c) The characteristics of development of the complex shock waves of the muzzle, owing to the constrained track, were notably different from those in its absence, with more pronounced fluctuations in the pressure at the monitoring points and the drag force on the moving body. The Mach number of the moving body was also higher than that in the model without the track.

Author Contributions: Z.L. performed the data analysis, conducted the formal analysis, and wrote the manuscript. H.W. performed the revision of the paper. All authors have read and agreed to the published version of the manuscript.

Funding: The evolution mechanism and control method of shock waves in a near ground constrained moving body under the impact of a dual bore jet, funded by the National Youth Science Foundation of China with grant numbers 124022682024.

Data Availability Statement: All data and models that support the findings of this study are available from the corresponding author upon reasonable request. All data and models generated or used during the study appear in the submitted article.

Acknowledgments: We thank Yonggang Yu for help with the written discussions in this paper.

Conflicts of Interest: The authors declare no conflicts of interest.

References

1. Jiang, S.; Wang, H.; Lin, C.; Wang, J. Establishment and simulation of two-dimensional interior ballistics model of large caliber Davis gun considering the axial movement of tubular charge clusters. *Acta Armamentarii* **2016**, *37*, 1941–1948. [CrossRef]
2. Wang, G.; Cheng, C.; Zhang, X.; Huang, X. Numerical simulation and analysis of muzzle flow during a rarefaction wave gun firing. *Propellants Explos. Pyrotech.* **2021**, *46*, 45–56. [CrossRef]
3. Goto, K.; Kato, Y.; Ishihara, K.; Matsuoka, K.; Kasahara, J.; Matsuo, A.; Funaki, I.; Nakata, D.; Higashino, K.; Tanatsugu, N. Thrust validation of rotating detonation engine system by moving rocket track test. *J. Propul. Power* **2020**, *37*, 419–425. [CrossRef]
4. Zhang, G.; Kim, H.D. Numerical simulation of shock wave and con tact surface propagation in micro shock tubes. *J. Mech. Sci. Technol.* **2015**, *29*, 1689–1696. [CrossRef]
5. Li, Z.J.; Wang, H. Effect of Precursor Flow Field of Muzzle on the Combustion Gas Jet Flow of Gun Propellant. *Chin. J. Energetic Mater.* **2017**, *25*, 282–290. [CrossRef]
6. Teramoto, S. Large-Eddy Simulation of Transitional Boundary Layer with Impinging Shock Wave. *AIAA J.* **2015**, *43*, 2354–2363. [CrossRef]
7. Mäkinen, T.; Pertilä, P. Shooter localization and bullet trajectory, caliber, and speed estimation based on detected firing sounds. *Appl. Acous.* **2010**, *71*, 902–913. [CrossRef]
8. Jones, A.R.; Medina, A.; Spooner, H.; Mulleners, K. Characterizing a burst leading-edge vortex on a rotating flat plate wing. *Exp. Fluids* **2016**, *57*, 1–16. [CrossRef]

9. Moumen, A.; Grossen, J.; Ndindabahizi, I.; Gallant, J.; Hendrick, P. Visualization and analysis of muzzle flow fields using the background-oriented schlieren technique. *J. Vis.* **2020**, *23*, 409–423. [CrossRef]
10. Florio, L.A. Effect of vent opening area and arrangement on gas flow field as gas propelled cylinder exits a flow tube. *Meccanica* **2010**, *45*, 475–501. [CrossRef]
11. Souverein, L.J.; Dupont, P.; Debiève, J.-F.; Dussauge, J.-P.; van Oudheusden, B.W.; Scarano, F. Effect of Interaction Strength on Unsteadiness in Shock-Wave-Induced Separations. *AIAA J.* **2010**, *48*, 1480–1493. [CrossRef]
12. Lees, L.; Reeves, B.L. Supersonic Separated and Reattaching Laminar Flows: I. General Theory and Application to Adiabatic Boundary Layer-Shock Wave Interactions. *AIAA J.* **2015**, *2*, 1907–1920. [CrossRef]
13. Schmidt, E.M.; Fansler, K.S.; Shear, D.D. Trajectory Perturbations of Fin-Stabilized Projectiles Due to Muzzle Blast. *J. Spacecr. Rocket.* **2015**, *14*, 339–344. [CrossRef]
14. Schmidt, E.M.; Shear, D. Optical measurements of muzzle blast. *AIAA J.* **2012**, *13*, 1086–1091. [CrossRef]
15. Guo, Z.Q.; Jiang, X.H.; Wang, Y. Parallel numerical simulation of muzzle reacting flow. *Chin. J. Comput. Mech.* **2013**, *30*, 111–116+123. [CrossRef]
16. Guo, Z.; Qiao, H.; Jiang, X. Numerical simulation on the characteristics of flow field of the muzzle of embedded aircraft gun. *Acta Armamentarii* **2017**, *38*, 2373–2378. [CrossRef]
17. Zhang, H.; Xiao, Y.; Zheng, C.; Chen, Z.; Xu, D.; Zhu, S.; Song, W. Characteristics of three-dimensional flow field structure of supersonic transverse jet. *J. Propul. Technol.* **2023**, *44*, 30–39. [CrossRef]
18. Zhang, H.; Chen, Z.; Jiang, X.; Li, H. Investigations on the exterior flow field and the efficiency of the muzzle brake. *J. Mech. Sci. Tech.* **2013**, *27*, 95–101. [CrossRef]
19. Li, Z.; Wang, H. Analysis of Ground Distance Effect on Hypervelocity Jet Flow and Stability of Projectile in Half-space. *AIP Adv.* **2022**, *12*, 045013. [CrossRef]
20. Li, Z.; Wang, H. Mechanism of Evolution of Shock Wave of Muzzle Jet under Initial Interference and Its Simplified Model. *Aerospace* **2024**, *11*, 381. [CrossRef]
21. Li, Z.; Wang, H.; Chen, J. Ground effects on the hypervelocity jet flow and the stability of projectile. *Eng. Appl. Comput. Fluid Mech.* **2018**, *12*, 375–384. [CrossRef]
22. Zhao, X.Y.; Zhou, K.D.; He, L.; Lu, Y.; Wang, J.; Zheng, Q. Numerical Simulation and Experiment on Impulse Noise in a Small Caliber Rifle with Muzzle Brake. *Shock Vib.* **2019**, *26*, 5938034. [CrossRef]

Disclaimer/Publisher's Note: The statements, opinions and data contained in all publications are solely those of the individual author(s) and contributor(s) and not of MDPI and/or the editor(s). MDPI and/or the editor(s) disclaim responsibility for any injury to people or property resulting from any ideas, methods, instructions or products referred to in the content.